TU Delft

Delft University of Technology

Measuring Bed Exchange Properties of Cohesive Sediments Using Tripod Data

Zhou, Z.; Ge, Jianzhong ; van Maren, D.S.; Gu, Jinghua; Ding, Pingxing; Wang, Zhengbing

DOI
10.3390/ jmse10111713

Publication date
2022

Document Version
Final published version

Published in
Journal of Marine Science and Engineering

Citation (APA)
Zhou, Z., Ge, J., van Maren, D. S., Gu, J., Ding, P., & Wang, Z. (2022). Measuring Bed Exchange Properties of Cohesive Sediments Using Tripod Data. *Journal of Marine Science and Engineering*, *10*(11). https://doi.org/10.3390/ jmse10111713

Important note
To cite this publication, please use the final published version (if applicable).
Please check the document version above.

Copyright
Other than for strictly personal use, it is not permitted to download, forward or distribute the text or part of it, without the consent of the author(s) and/or copyright holder(s), unless the work is under an open content license such as Creative Commons.

Takedown policy
Please contact us and provide details if you believe this document breaches copyrights.
We will remove access to the work immediately and investigate your claim.

This work is downloaded from Delft University of Technology.
For technical reasons the number of authors shown on this cover page is limited to a maximum of 10.

Journal of *Marine Science and Engineering*

MDPI

Article

Measuring Bed Exchange Properties of Cohesive Sediments Using Tripod Data

Zaiyang Zhou [1,2], Jianzhong Ge [1,3], Dirk Sebastiaan van Maren [1,2,4,*], Jinghua Gu [1], Pingxing Ding [1] and Zhengbing Wang [2,4]

[1] State Key Laboratory of Estuarine and Coastal Research, East China Normal University, Shanghai 200241, China
[2] Faculty of Civil Engineering and Geosciences, Delft University of Technology, 2628 CN Delft, The Netherlands
[3] Institute of Eco-Chongming (IEC), No. 20 Cuiniao Road, ChenJiazhen, Shanghai 202162, China
[4] Department of Marine and Coastal Systems, Deltares, 2600 MH Delft, The Netherlands
* Correspondence: bas.vanmaren@deltares.nl

Abstract: The Krone–Partheniades (K-P) framework has been used for decades to quantify and analyze the sediment exchange at a water–bed interface. Measuring the erosion and deposition parameters that are part of this framework requires time-consuming field observations. Additionally, the erosion parameters are measured independently of deposition parameters, while in reality they are coupled. In numerical models applying the K-P framework these parameters are often assumed to be constant in time and mutually independent. In this study, we develop a relatively simple methodology to determine the erosion and deposition parameters, using conventional near-bed observations of bed level, sediment concentration and flow velocity. This methodology is subsequently applied to tripod observations collected in the Changjiang estuary, China, to compute continuous time-varying erosion and settling parameters. We propose a diagram to visualize the interdependency and accuracy of erosion and deposition parameters, which is the input for K-P framework models requiring this interdependency.

Keywords: Krone–Partheniades equations; observations techniques; settling velocity; critical shear stress

check for updates

Citation: Zhou, Z.; Ge, J.; van Maren, D.S.; Gu, J.; Ding, P.; Wang, Z. Measuring Bed Exchange Properties of Cohesive Sediments Using Tripod Data. *J. Mar. Sci. Eng.* **2022**, *10*, 1713. https://doi.org/10.3390/jmse10111713

Academic Editor: Antoni Calafat

Received: 11 October 2022
Accepted: 3 November 2022
Published: 10 November 2022

Publisher's Note: MDPI stays neutral with regard to jurisdictional claims in published maps and institutional affiliations.

Copyright: © 2022 by the authors. Licensee MDPI, Basel, Switzerland. This article is an open access article distributed under the terms and conditions of the Creative Commons Attribution (CC BY) license (https://creativecommons.org/licenses/by/4.0/).

1. Introduction

The well-known Krone–Partheniades (K-P) bed level change model [1–4] is widely applied in numerical models to quantitatively describe the morphodynamics of muddy environments. However, this model also has several shortcomings in its application (especially in numerical models), the most important ones probably being that erosion and deposition parameters are (1) assumed to be constant in time, and (2) site-specific and difficult to measure.

The complexity of most physical environments implies that the parameters in the K-P formula are variable in time on the timescale of minutes (due to deposition and dewatering of fresh sediments) to seasons (due to biological effects or the erosion of a heterogeneous substrate). Numerical models applying the K-P equations usually assume constant input parameters [5–8], although they may vary over space [9] and time due to, e.g., consolidation [10–12]. The assumption of constant parameters is especially wrong during episodic high-energy events such as river floods or storm events, when bed erosion leads to the exposure of more consolidated, deeper layers.

Secondly, measuring deposition and erosion parameters with conventional methods is laborious and sometimes impossible. This is related to the fragile structure of fine sediments, coagulating into flocs with different settling and erosion properties compared to the individual particles. This introduces temporal variations in sediment properties, complicating sample analysis in laboratories. Many methodologies additionally affect

turbulent shear, destroying flocs and thereby influencing the settling velocity. Full in-situ observations of settling velocity (using floc cameras, such as [13–15]) and erosion rates under submerged conditions (the sea bed carrousel by [16] or laboratory analysis on in situ collected cores by [17]) are very time-consuming and expensive. Erosion and deposition parameters are additionally measured separately, sometimes over considerable horizontal distances.

To advance our knowledge on near-bed sediment dynamics and improve the parameterizations of erosion/deposition processes, there is a need for continuous (and therefore simultaneous) observations of erosion and deposition properties. In this paper, we introduce a methodology to derive such parameters through analysis of simultaneous observations of hydrodynamic properties and bed level changes.

2. Methods

2.1. Field Measurements

We conducted in situ observations with a near-bed tripod system in the North Passage (NP, the main navigation channel) of the Changjiang estuary (Figure 1). The suspended sediment concentration (SSC) in the NP can be up to tens of kg/m^3 in the form of concentrated benthic suspension [18]. The seabed of the NP mainly consists of fine sediment; the medium grain sizes (d_{50}) at our observational site are between 20 and 50 μm, with a high clay content of about 20–30% [19]. The seabed seaward of the observational site is even more fine-grained (d_{50} < 10 μm with a clay content > 35%).

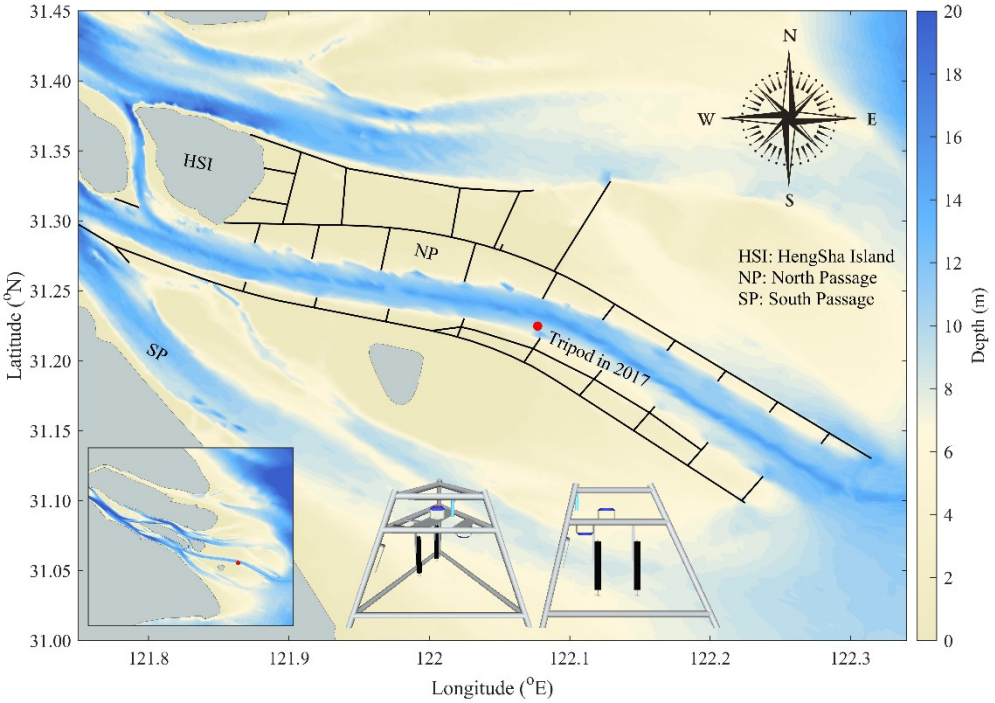

Figure 1. Bathymetry of the North Passage and adjacent regions. Black lines in the river mouth represent dikes and groins around the North Passage. Red dots indicate the measuring site in 2017. The insets show the bathymetry of the whole Changjiang estuary, and the tripod system used for near-bed observations.

Field observations were conducted in the NP from 2 July to 15 July 2017 (during the peak of the monsoon period) using a tripod system at a water depth of about 10 m (see Table 1 for details). No information is available on scour and deposition around the frame as a result of its deployment. The Suspended Sediment Concentration (SSC) was measured with an Optical Back Scatter sensor mounted 0.9 m above the bed (mab); the velocity was measured using two RDI Acoustic Doppler Current Profilers (ADCPs), two

Nortek Acoustic Doppler Vectors (ADVs) and a JFE ALEC Point Current Meter (PCM). The ADVs also measure the distance between the probe and the bed (D), from which a relative bed level (RBL) can be computed as:

$$RBL_{observed} = \overline{D} - D \quad (1)$$

where the overbar denotes the time-averaged value. An increasing trend of the RBL indicates deposition (and a decreasing trend erosion). The upward-looking ADCP was also used to compute wave height and period. These tripod observations are used to compute erosion parameters and the sediment settling parameters in the K-P model, as elaborated in the following sections.

Table 1. Instruments mounted on the tripod and their sampling configurations.

Instrument Deployed	Distance above Bed (m)	Sampling Interval (min)	Sampling Configuration	Survey Parameter
ADCP upward	1.2	/	120 s (1 h for wave observation)	Profile velocity, waves
ADCP downward	1.0	/	120 s	Profile velocity
PCM	1.15	2	0.2 Hz (every first 50 s)	Velocity
ADV	0.25	10	16 Hz (every first 70 s)	Near-bed velocity
OBS	0.9	/	100 s	Salinity, temperature, turbidity, pressure

2.2. The K-P Model and Data Processing

The erosion M_e and deposition M_d rates (both in kg/(m^2s)) are calculated using [1–3,20]:

$$\frac{dM_e}{dt} = \begin{cases} m_e\left(\frac{\tau-\tau_{ce}}{\tau_{ce}}\right), & \tau > \tau_{ce} \\ 0, & \tau \le \tau_{ce} \end{cases} \quad (2)$$

$$\frac{dM_d}{dt} = -c_b w_{s,b} \quad (3)$$

where m_e (kg/(m^2s)) and τ_{ce} (N/m^2) are the erosion coefficients and critical shear stress for erosion, respectively; $w_{s,b}$ is the settling velocity (m/s); τ represents the bed shear stress (N/m^2) and c_b (kg/m^3) denotes the bottom sediment concentration. The bed shear stress τ is calculated with the Grant–Madsen method [21] using ADCP observations (see below). The bottom sediment concentration c_b is measured with a calibrated OBS, and used to correct $w_{s,b}$ for hindered settling using [22]:

$$w_{s,b} = w_{s,0}\frac{(1-\phi)^m(1-\phi_p)}{1+2.5\phi} \quad (4)$$

where $w_{s,0}$ is the settling velocity in clear water; $\phi = c_b/c_{gel}$ is the volumetric sediment concentration; $\phi_p = c_b/\rho_s$ is the volumetric primary particle concentration, ρ_s is the density of sediment 2650 kg/m^3; m represents non-linear effects for which we use m = 2 (following [23]), and c_{gel} is specified as 250 kg/m^3 (based on settling observations with Yangtze sediment, to which Equation (4) was fitted [24] and in line with [9]). The cumulative relative bed level (from t_0 to T) can be computed by integrating the erosion and deposition rates at each time step:

$$RBL_{simulated} = \sum_{t_0}^{T}\left(\frac{dM_d}{dt} - \frac{dM_e}{dt}\right)\Delta t/\rho_d \quad (5)$$

where ρ_d is the dry density, assumed (in absence of observations) to be 1300 kg/m^3 because of the high silt content; Δt is the time step (= 1 h in this study). The K-P model is therefore driven by measured values for c_b and τ, while m_e, τ_{ce}, and $w_{s,0}$ ($w_{s,b}$) remain to be determined by simultaneously fitting both Equations (2) and (3) to observed bed level changes.

2.3. The Bed Shear Stress

The bed shear stress can be computed using the ADCP observations (using the Grant–Madsen model [21]—hereafter referred to as GM94) and the ADVs (using the turbulent kinetic energy or TKE method). The GM94 method assumes a logarithmic velocity profile over rough beds and hence a well-mixed water column. The assumption of hydraulically rough flow can be evaluated with the roughness Reynolds number $\mathrm{Re}_* = u_* k_s / v$ with u_* being the bed shear velocity, k_s the Nikkuradse roughness height, and v the kinematic viscosity. For $\mathrm{Re}_* > 70$, the flow is hydraulically rough and the bed roughness height is constant, depending on bed properties (as in GM94). For conditions typical for the North Passage, with strong tidal flow velocities up to 1.5 m/s, the assumption of hydraulically rough flow is valid throughout the tidal cycle, except for a very short period around slack tide. However, the Changjiang Estuary is both salinity- and sediment-stratified, violating the assumption of a well-mixed water column and a fully logarithmic velocity profile. Therefore, the TKE method is more suitable from a physical point of view. Unfortunately, the ADVs malfunctioned more often than the ADCP, so ADCP-derived bed shear stresses would expand the available dataset. We therefore intercompare both methods, and when yielding similar results continue with the GM94 method.

The current induced bed shear stress (τ_c) in the GM94 method is calculated as:

$$\tau_c = \rho_w (u_{*c})^2 \tag{6}$$

The original GM94 method allows for a wave-induced and flow-induced contribution to the bed shear stress. With a water depth of 10 m and a wave height of 0.3 m, the wave orbital velocity is very low (several cm/s), and as a result the wave-induced bed shear stress is negligible compared to the current-induced bed shear stress (see Figure 2, in which both the wave-induced and current-induced bed shear stress are computed using [21]).

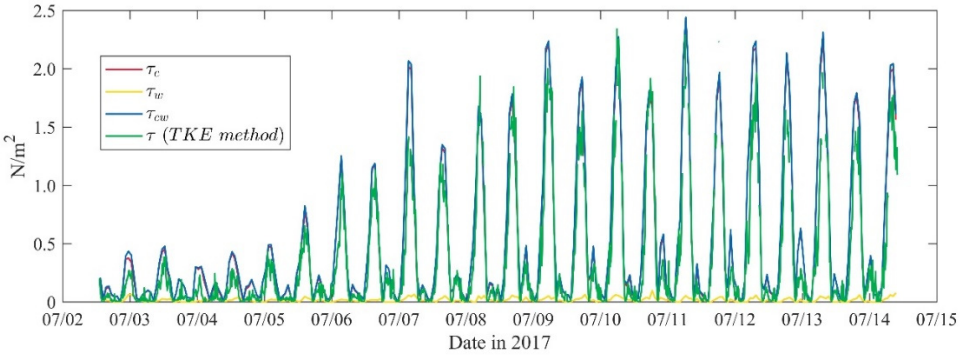

Figure 2. Calculation of bed shear stress, comparison between Grant–Madsen method and the TKE method. The red and blue lines largely overlap because the wave-induced shear stress (yellow line) is very small.

The TKE method computes the turbulent kinetic energy measured at 0.25 m above the bed by the ADV, as in

$$TKE = \frac{1}{2}\rho\left(\overline{u'^2} + \overline{v'^2} + \overline{w'^2}\right) \tag{7}$$

where u', v', w' are fluctuating velocity components in the XYZ coordinates relative to a 70 s averaged value with a burst of 10 min, the overbar denoting time-averaging. The

TKE method is not subject to the error related to the sensor height z [25] and therefore the TKE-based bed shear stress can be calculated with the equation:

$$\tau = C \cdot TKE \quad (8)$$

where C is a proportionality constant, which is 0.19 [26] to 0.20 [27]—we assumed $C = 0.19$.

The resulting time-varying τ is remarkably similar when using both methods (Figure 2). This suggests that the assumed bed roughness for the GM94 method is reasonable, and deviations from the logarithmic velocity profile are sufficiently low to use the GM94 method (which is preferable from a practical point of view, given the larger availability of ADCP data).

2.4. Data Fitting Methodology

The values for m_e, τ_{ce}, and $w_{s,b}$ are determined through a semi-automatic least-squares fitting method against observational data. Over a user-specified time window of length T and within a user-defined range and interval of unknown input parameters (m_e, τ_{ce}, and $w_{s,0}$), a large number of K-P model realizations are executed with a MATLAB model. These realizations include all possible combinations of the three variable parameters within their user-prescribed range (i.e., ten potential values for m_e and τ_{ce}, as well as $w_{s,0}$, result in 1000 model realizations for that particular time window). Within the time window, the accuracy of each predicted bed level ($RBL_{simulated}$) is quantified with a correlation coefficient (R^2) and Root Mean Square Error (RMSE) using the measured bed level changes ($RBL_{observed}$). The parameter set with the highest correlation coefficient is defined as most representative within the evaluated time window T (see Figure 3). The time window then shifts forward in time with ΔT to run the model for the same amount of input parameter combinations. Note that $\Delta T < T$, resulting in a more gradual change in input parameters compared to a simple piecewise segmentation with the time window T.

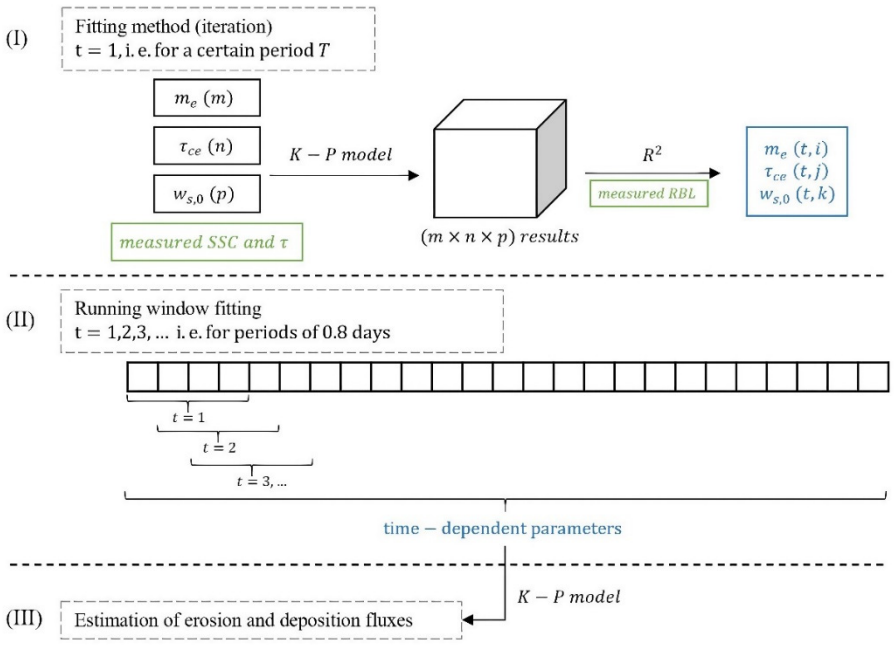

Figure 3. Schematized procedure for data fitting. The general approach (**I**) is to compute a large number of possible relative bed levels (*RBL*), realized with a range of K-P model settings, by varying τ_{ce}, m_e, and/or $w_{s,0}$, and fitting these to observed *RBL* using an R^2. Then the approach is repeated with a running window fitting method (**II**), providing a timeseries of freely varied input parameters. These time-varying parameters are subsequently used to compute erosion and deposition fluxes (**III**).

This method allows for the free-fitting of all three parameters, but also for assuming one or two input parameters as constant. For instance, for every combination of constant τ_{ce} and m_e, the time-dependent $w_{s,0}$ can be computed with the running window fitting according to the highest R^2. As a result, a time-varying $w_{s,0}$, RMSE, and R^2 are obtained for each combination of constant τ_{ce} and m_e.

3. Observational Data

3.1. General Observations

The river discharge increased during the observational period, reaching 7×10^4 m^3/s on 07/10 (nearly twice the average wet season discharge) (see Figure 4a), resulting in ebb-dominant conditions (higher ebb flow velocities and a longer duration of ebb flows). The tidal currents during spring tides were 2 to 2.5 times higher than neap tide currents (Figure 4b).

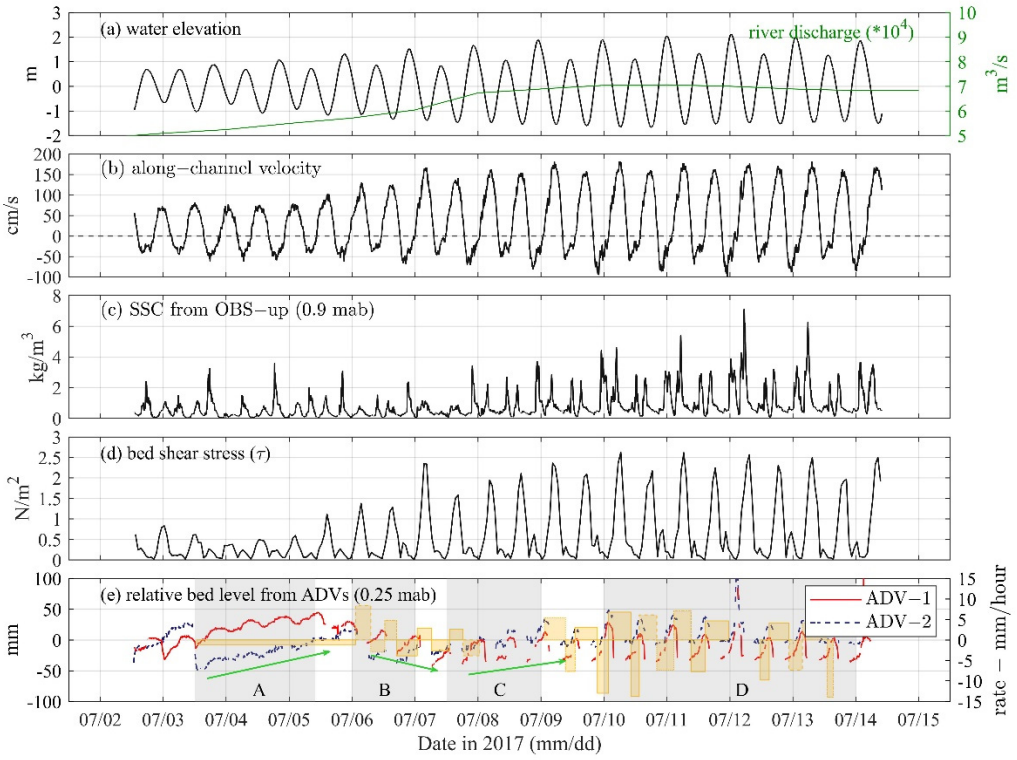

Figure 4. Observed variables: (**a**) discharge (Datong Gauge Station, 600 km upstream) and water elevation (OBS), (**b**) along-channel current velocity (ALEC), (**c**) suspended sediment concentration (SSC), (**d**) bed shear stress, and (**e**) relative bed level and the rate of bed level changes (ADV). The positive values of along-channel current velocity denote ebb currents.

The SSC peaked during each ebb and flood (Figure 4c) and was higher during and after the spring tide resulting from either advection (due to higher river discharge) or resuspension (due to higher bed shear stress) (Figure 4a,d). The bed shear stress during neap tidal conditions was low (<0.5 N/m^2) compared to spring tidal conditions (2.5 N/m^2; Figure 4d). This pronounced difference in hydrodynamic forcing is reflected in the patterns of bed level changes (the *RBL* measured by two ADVs, Figure 4e). Both ADVs recorded similar bed level changes, although the break in the ADV-2 data on 07/03 is probably the result of a mass movement of sediment (a local sediment slide or turbidity current), which rapidly changed the bed level but did not tilt the measurement frame. With ADV-1 (red line in Figure 4e) producing the longest timeseries of bed level change, we use ADV-1 for the analysis hereafter.

3.2. Sediment Dynamics

The observations in Figure 4e reveal four stages with distinct erosion and sedimentation characteristics. Stage A (neap tide) was characterized by persistent deposition, whereas phases B–D by alternating periods of erosion and sedimentation. Net erosion prevailed during phase B, while net sedimentation prevailed during phase C; phase D was in equilibrium. Next, we evaluate the role of resuspension and advection processes by relating SSC to $u|u|$ (Figure 5, u is the longitudinal flow velocity positive in the ebb current direction). During neap tides (line of 07/07, as an example), the ebb SSC remained quite low (even at moderately high $u|u|$). During moderate and spring tides (lines of 07/08 to 07/13), the SSC increased with $u|u|$ for $u|u| > 0.5$ m^2/s^2 (suggesting local resuspension), but decreased before the maximum of $u|u|$ was achieved (suggesting sediment advection). The increase in SSC with $u|u|$ was stronger during spring tides than during neap tides, suggesting local resuspension to be dominant. It is likely that the amount of sediment available for erosion is limited (by advective processes), but the actual SSC is still strongly governed by local sediment resuspension. During flood tide, the $u|u|$ was below 0.5 m^2/s^2, and therefore no clear pattern in SSC exists. The erosion and deposition parameters obtained from our local erosion and deposition model are therefore more accurate during spring tide ebb conditions (especially the beginning of ebb), but less accurate during neap tides and flood tides. The fitting procedure introduced in this paper is therefore especially valid for the period 8–13 July, and less outside this specific period.

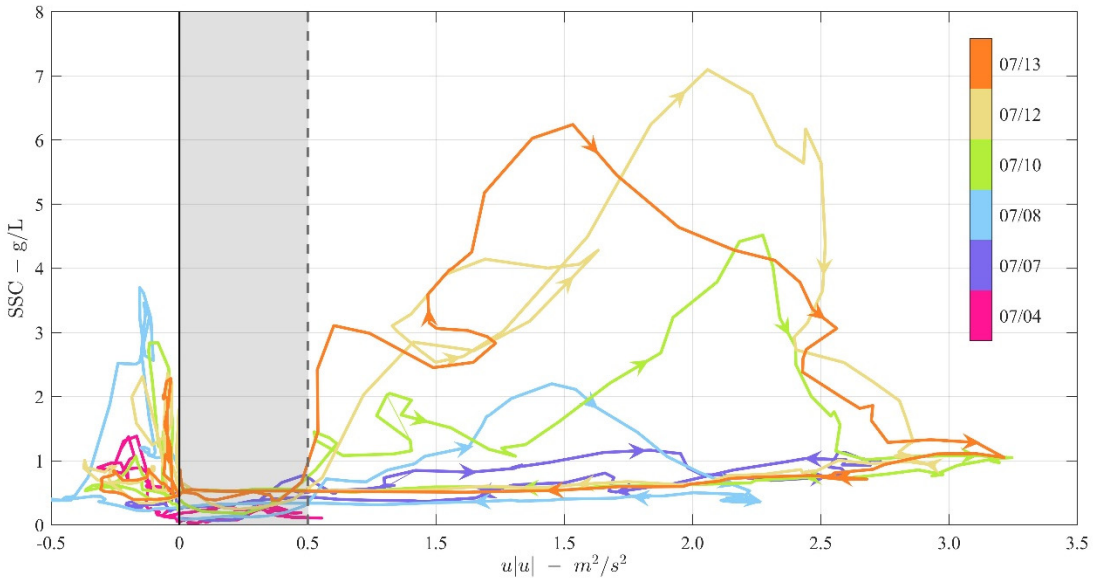

Figure 5. Variation in SSC against the square velocity within each tidal cycle. $u|u| > 0$ indicates the ebb tide.

4. A parameter Space Diagram for the K-P Formulations

The erosion flux is composed of the erosion parameter m_e and the critical erosion shear stress τ_{ce}. Within a given distribution of bed shear stress, multiple combinations of m_e and τ_{ce}, provide the same integrated erosion flux. Similarly, the erosion flux balances the deposition flux, where again for a given bed shear stress, sediment concentration and settling velocity, multiple combinations of m_e, τ_{ce}, and $w_{s,0}$ exist, which create comparable bed level variability.

The semi-automatic fitting method computes a time-varying $w_{s,0}$ for each combination of constant τ_{ce} and m_e (Section 2), and the model is run for a large range of constant τ_{ce} and m_e. By averaging $w_{s,0}$ for each model realization and computing the RMSE and R^2, the performance of each combination of τ_{ce}, m_e, and $w_{s,0}$ can be evaluated in a parameter space diagram (Figure 6). This diagram provides the interdependency of all erosion and

deposition flux parameters, as well as their goodness-of-fit against observational data. For instance, the diagram reveals that a τ_{ce} of 0.1 N/m^2 requires an m_e of (approximately) 0.6, 1.8, 2.8, and 3.8 $\times$ 10^{-4} kg/(m^{2}s) for a settling velocity of 0.5, 1.0, 1.5, and 2.0 mm/s, respectively. The accuracy of these parameter combinations is evaluated with R^2 and RMSE, which are both contoured in the same parameter space diagram, attaining a maximum R^2 of 0.65 and minimum RMSE of 8 mm for a $w_{s,0}$ between 1.5 and 2 mm/s.

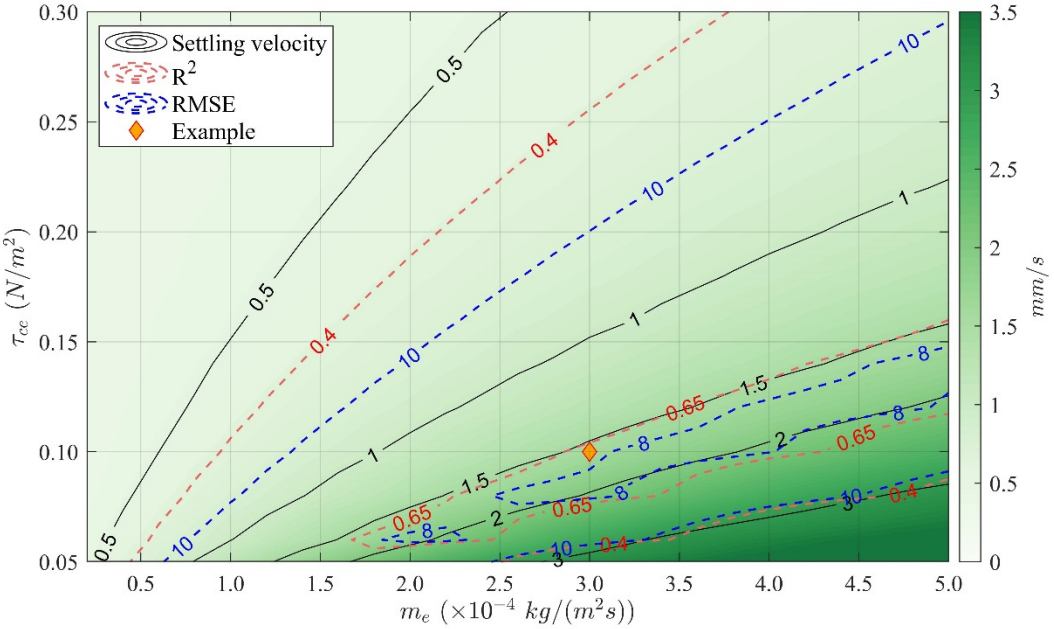

Figure 6. Average value of fitted $w_{s,0}$ (black contours) as a function of τ_{ce} and m_e. The red and blue dashed lines indicate contours of averaged R^2 and RMSE (R^2 and RMSE are time-varying in the running window fitting). The diamond-shape marker denotes an example of parameterized τ_{ce}, m_e, and $w_{s,0}$ (1.6 mm/s).

Figure 7 exemplifies time series of the data fitting for the parameter settings corresponding to the diamond-shape mark in Figure 6 (m_e = 3 $\times$$10^{-4}$ kg/(m^{2}s), τ_{ce} = 0.1 N/m^2, and $w_{s,0}$ = 1.6 mm/s). The fit with constant parameters captures the main characteristics of the measured *RBL* (Figure 7a), indicating that the parameter space diagram is a useful tool to rapidly determine the required parameters (for instance, as input for numerical models). Obviously, allowing all parameters to vary over time (blue lines in Figure 7) generates a much better fit to the observations. The value of such free fitting will be explored in more detail in the next section.

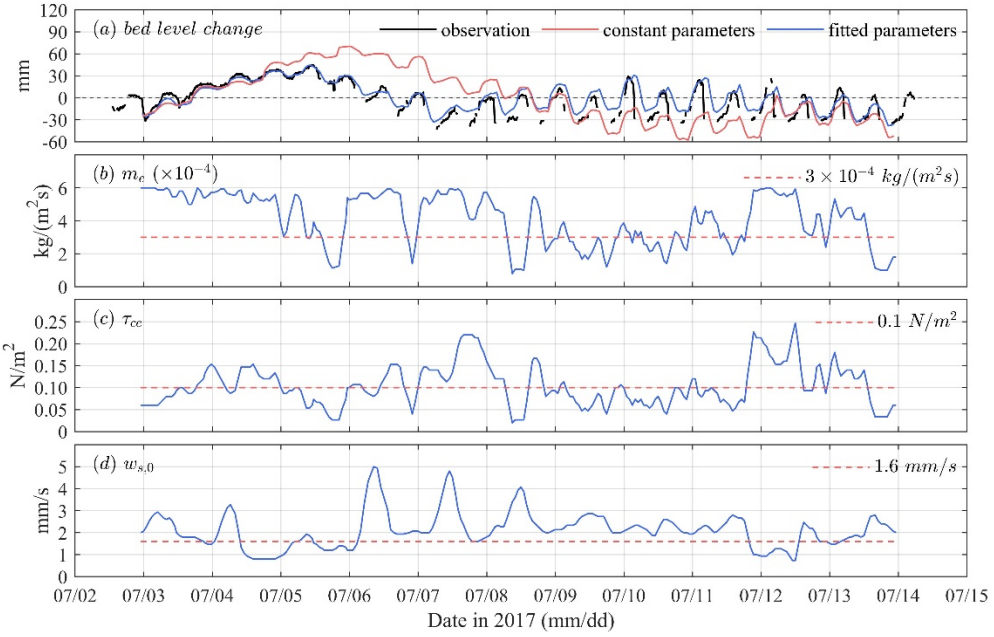

Figure 7. (**a**) Comparison between measured *RBL* (ADV-1) and simulated *RBL* using constant (red) and time-varying (blue) parameters, (**b**–**d**) constant and time-varying m_e, τ_{ce}, and $w_{s,0}$. Parameters presented here are smoothed using a three-hour moving average and the *RBL* (blue) is computed using the smoothed parameters.

5. Discussion

The free-fitted, time-varying erosion and deposition fluxes fluctuate within a realistic parameter space. $w_{s,0}$ was mainly in the range of 1–3 mm/s, corresponding well with in situ observations of floc settling velocities elsewhere [13,15]. With the substrate being composed of muddy sediments (d_{50} between 20 and 50 µm, corresponding to a single particle settling velocity between 0.1 and 1 mm/s) the computed settling velocities between 1 and 3 mm/s imply the suspended sediments are flocculated. The critical shear stress for erosion τ_{ce} was varied between 0.05 and 0.15 N/m^2 indicating soft, easily erodible surface mud layers [17,28,29]. The erosion parameter m_e was more variable, ranging between 1 and 6 $\times 10^{-4}$ kg/(m^{2}s), which is in agreement with the typical range of 0.1 to 5 $\times 10^{-4}$ kg/(m^{2}s) provided by [30].

The temporal variability of the fitted parameters allows a more in-depth analysis of the suspended sediment dynamics. For example, the critical shear stress in Figure 7c was lower during a period of deposition from 07/03 to 07/05 (average value of 0.11 N/m^2) than that during an overall erosion period from 07/06 to 07/08 (average value of 0.14 N/m^2), which is consistent with freshly deposited sediments being more easily erodible. Therefore, the proposed method provides an alternative to conventional field observation techniques, such as in situ erosion measurements [31], laboratory analysis on sediment cores [17], or flocculation cameras [13,15], which are much more costly and do not generate full time series of sediment properties. Furthermore, our methodology has been applied in a very turbid environment, which is challenging for optic instruments measuring the settling velocity.

A disadvantage of our methodology is that it may lead to the frequent switching of free-fitted parameters. This is because our hourly bed level changes reflect net bed level changes (rather than gross bed level changes, which may occur in much smaller time periods) and multiple parameter combinations may exist, which may describe the bed level evolution with a very similar correlation (non-uniqueness or equifinality [32]). Within the K-P framework, equifinality arises from (1) the balance between the deposition flux ($w_{s,0}$) and the erosion flux (τ_{ce} and m_e) in defining the net bed level change, and (2) the balance between τ_{ce} and m_e in defining the erosion flux. Multiple parameter sets can therefore lead

to a similar R^2, and small changes in R^2 may lead to the frequent and irregular switching from one parameter set to another. Within our procedure, this irregular switching in input parameters resulting from non-uniqueness can be minimized by using a longer running window T (in which the fitted parameters are assumed to be constant). The best model fit is therefore a balance between an overly averaged solution and a rapidly alternating solution resulting from equifinality, resulting in a time window T of 0.8 days.

The parameter space diagram provides a novel methodology to develop numerical fine sediment transport models more quickly, but also more accurately. The temporal variation in sediment properties (Figure 7) as observed from the tripod may provide more in-depth understanding of the sediment dynamics, which may lead to better models when increasing the complexity of the model (through, e.g., consolidation, flocculation or biophysical interactions). However, its greatest value for improving the numerical model is related to the relations between K-P parameters, as visualized in Figure 6. This diagram provides a realistic set of (initial) input parameters, reducing the time required for model calibration. The method leads to more accurate models because it allows the detailed (and much faster) exploration of non-uniqueness, introduced above via parameter switching.

Non-uniqueness or equifinality may be useful for quantifying the accuracy of model predictions, especially outside its calibration space [32]; for instance, conditions of extreme sea level rise or channel deepening. For this purpose, a number of models with equifinal model input parameters need to be developed and run within and beyond its calibration space. When the predicted bed level changes are similar for a range of equifinal parameter sets for conditions outside the original calibration space, the model can be considered to be only narrowly influenced by equifinality (and hence model parameter values), and therefore robust and accurate. Developing such equifinal input parameter combinations is a time-consuming process. However, our parameter space diagram provides a methodology to rapidly develop alternative model input settings, thereby enabling the use of equifinality as a tool to quantify the accuracy of future predictions.

Although we believe our methodology provides an important step in understanding and quantifying near-bed sediment dynamics, our method may be improved in several aspects. First, we used suspended sediment concentration (at about 0.9 mab) as the bottom sediment concentration. Although the observed "near-bottom" SSC and the actual concentration close to the bed are related, the actual near-bed SSC is higher. Future work should aim at deploying the turbidity sensor at a lower position. Another limitation is the assumption of a single class of sediment. In our study area, the sea bed is mainly composed of fine cohesive sediments with spatial and temporal variability in sediment compositions and properties. The method proposed in this study cannot distinguish the distribution of sediment properties because it would introduce too many degrees of freedom in the fitting procedure. Accounting for such distributions would require additional instrumentation aiming at continuously measuring a proxy for the settling velocity, such as a LISST (measuring the grain size distribution [33]) or ADV (converting turbulent fluctuations into a settling flux [34]). Such parallel observations would also provide calibration data for our methodology and reduce the impact of equifinality.

6. Conclusions

A methodology is developed to compute erosion and settling properties (m_e, τ_{ce}, and $w_{s,0}$) using standard tripod observations (measuring flow velocity, SSC, and bed level). A least-squares fitting method is deployed to compute time-varying and constant sediment parameter sets. This methodology accounts for the interrelationships between settling and deposition, which can be conveniently visualized in a m_e–τ_{ce}–$w_{s,0}$ diagram. By additionally computing the accuracy of the fit (using RMSE and R2), this methodology provides a much better estimation for erosion/deposition parameters than existing methodologies, especially for use in numerical models. It additionally provides a method to evaluate the time variation of erosion and deposition parameters.

Author Contributions: Conceptualization: Z.Z. and D.S.v.M.; methodology: Z.Z. and J.G. (Jianzhong Ge); software development: Z.Z.; data collection: J.G. (Jianzhong Ge), J.G. (Jinghua Gu) and P.D.; writing: Z.Z., J.G. (Jianzhong Ge), D.S.v.M. and Z.W.; funding acquisition: J.G. (Jianzhong Ge) and P.D. All authors have read and agreed to the published version of the manuscript.

Funding: This research is supported by the National Natural Science Foundation of China (Grant No. 41776104) and KNAW Project (Grant PSA-SA-E-02).

Institutional Review Board Statement: Not applicable.

Informed Consent Statement: Not applicable.

Data Availability Statement: All data sets used in this study are publicly available at https://figshare.com/s/edbb8f8c27654c1b1d70, accessed on 1 November 2022.

Acknowledgments: We acknowledge the suggestions by two anonymous reviewers for improving the quality of this paper.

Conflicts of Interest: The authors declare no conflict of interest.

References

1. Ariathurai, C.R. *A Finite Element Model for Sediment Transport in Estuaries*; University of California, Davis: Davis, CA, USA, 1974.
2. Krone, R.B. *Flume Studies of the Transport of Sediment in Estuarial Shoaling Processes: Final Report*; Hydraulic Engineering Laboratory and Sanitary Engineering Research Laboratory, University of California: Berkeley, CA, USA, 1962.
3. Partheniades, E.A. Erosion and Deposition of Cohesive Soils. *J. Hydraul. Div.* **1965**, *1*, 190–192. [CrossRef]
4. Winterwerp, J.C.; van Kesteren, W.G.M. *Introduction to the Physics of Cohesive Sediment Dynamics in the Marine Environment*; Elsevier: Amsterdam, The Netherlands, 2004; ISBN 0444515534.
5. de Nijs, M.A.J.; Pietrzak, J.D. Saltwater Intrusion and ETM Dynamics in a Tidally-Energetic Stratified Estuary. *Ocean Model* **2012**, *49–50*, 60–85. [CrossRef]
6. Sanford, L.P.; Halka, J.P. Assessing the Paradigm of Mutually Exclusive Erosion and Deposition of Mud, with Examples from Upper Chesapeake Bay. *Mar. Geol.* **1993**, *114*, 37–57. [CrossRef]
7. van Maren, D.S.; Winterwerp, J.C.; Wu, B.S.; Zhou, J.J. Modelling Hyperconcentrated Flow in the Yellow River. *Earth Surf. Process. Landf.* **2009**, *34*, 596–612. [CrossRef]
8. Dijkstra, Y.M.; Schuttelaars, H.M.; Schramkowski, G.P.; Brouwer, R.L. Modeling the Transition to High Sediment Concentrations as a Response to Channel Deepening in the Ems River Estuary. *J. Geophys. Res. Ocean.* **2019**, *124*, 1578–1594. [CrossRef]
9. Ge, J.; Shen, F.; Guo, W.; Chen, C.; Ding, P. Estimation of Critical Shear Stress for Erosion in the Changjiang Estuary: A Synergy Research of Observation, GOCI Sensing and Modeling. *J. Geophys. Res. Ocean.* **2015**, *120*, 8439–8465. [CrossRef]
10. Sanford, L.P. Modeling a Dynamically Varying Mixed Sediment Bed with Erosion, Deposition, Bioturbation, Consolidation, and Armoring. *Comput. Geosci.* **2008**, *34*, 1263–1283. [CrossRef]
11. Zhou, Z.; van der Wegen, M.; Jagers, B.; Coco, G. Modelling the Role of Self-Weight Consolidation on the Morphodynamics of Accretional Mudflats. *Environ. Model. Softw.* **2016**, *76*, 167–181. [CrossRef]
12. Winterwerp, J.C.; Zhou, Z.; Battista, G.; Van Kessel, T.; Jagers, H.R.A.; Van Maren, D.S.; Van Der Wegen, M. Efficient Consolidation Model for Morphodynamic Simulations in Low-SPM Environments. *J. Hydraul. Eng.* **2018**, *144*, 04018055. [CrossRef]
13. Manning, A.J.; Dyer, K.R. Mass Settling Flux of Fine Sediments in Northern European Estuaries: Measurements and Predictions. *Mar. Geol.* **2007**, *245*, 107–122. [CrossRef]
14. Smith, S.J.; Friedrichs, C.T. Size and Settling Velocities of Cohesive Flocs and Suspended Sediment Aggregates in a Trailing Suction Hopper Dredge Plume. *Cont. Shelf Res.* **2011**, *31*, S50–S63. [CrossRef]
15. Soulsby, R.L.; Manning, A.J.; Spearman, J.; Whitehouse, R.J.S. Settling Velocity and Mass Settling Flux of Flocculated Estuarine Sediments. *Mar. Geol.* **2013**, *339*, 1–12. [CrossRef]
16. Amos, C.L.; Grant, J.; Daborn, G.R.; Black, K. Sea Carousel-A Benthic, Annular Flume. *Estuar. Coast. Shelf Sci.* **1992**, *34*, 557–577. [CrossRef]
17. Dickhudt, P.J.; Friedrichs, C.T.; Sanford, L.P. Mud Matrix Solids Fraction and Bed Erodibility in the York River Estuary, USA, and Other Muddy Environments. *Cont. Shelf Res.* **2011**, *31*, S3–S13. [CrossRef]
18. Ge, J.; Zhou, Z.; Yang, W.; Ding, P.; Chen, C.; Wang, Z.B.; Gu, J. Formation of Concentrated Benthic Suspension in a Time-Dependent Salt Wedge Estuary. *J. Geophys. Res. Ocean.* **2018**, *123*, 8581–8607. [CrossRef]
19. Ge, J.; Chen, C.; Wang, Z.B.; Ke, K.; Yi, J.; Ding, P. Dynamic Response of the Fluid Mud to a Tropical Storm. *J. Geophys. Res. Ocean.* **2020**, *125*, e2019JC015419. [CrossRef]
20. Whitehouse, R.; Soulsby, R.; Roberts, W.; Mitchener, H. *Dynamics of Estuarine Muds*; Thomas Telford Publishing: London, UK, 2000; ISBN 0-7277-3762-7.
21. Madsen, O.S. Spectral Wave-Current Bottom Boundary Layer Flows. In Proceedings of the Coastal Engineering 1994, Kobe, Japan, 23–28 October 1994; American Society of Civil Engineers: New York, NY, USA, 1994; pp. 384–398.

22. Dankers, P.J.T.; Winterwerp, J.C.; van Kesteren, W.G.M. A Preliminary Study on the Hindered Settling of Kaolinite Flocs. In *Proceedings in Marine Science*; Elsevier: Amsterdam, The Netherlands, 2007; Volume 8, pp. 227–241. ISBN 9780444521637.
23. Dankers, P.J.T.; Winterwerp, J.C. Hindered Settling of Mud Flocs: Theory and Validation. *Cont. Shelf Res.* **2007**, *27*, 1893–1907. [CrossRef]
24. te Slaa, S.; He, Q.; van Maren, D.S.; Winterwerp, J.C. Sedimentation Processes in Silt-Rich Sediment Systems. *Ocean Dyn.* **2013**, *63*, 399–421. [CrossRef]
25. Kim, S.-C.; Friedrichs, C.T.; Maa, J.P.-Y.; Wright, L.D. Estimating Bottom Stress in Tidal Boundary Layer from Acoustic Doppler Velocimeter Data. *J. Hydraul. Eng.* **2000**, *126*, 399–406. [CrossRef]
26. Soulsby, R.L. The Bottom Boundary Layer of Shelf Seas. In *Physical Oceanography of Coastal and Shelf Seas*; Johns, B., Ed.; Elsevier: Amsterdam, The Netherlands, 1983; Volume 35, pp. 189–266.
27. Soulsby, R.L.; Dyer, K.R. The Form of the Near-Bed Velocity Profile in a Tidally Accelerating Flow. *J. Geophys. Res.* **1981**, *86*, 8067. [CrossRef]
28. Widdows, J.; Friend, P.L.; Bale, A.J.; Brinsley, M.D.; Pope, N.D.; Thompson, C.E.L. Inter-Comparison between Five Devices for Determining Erodability of Intertidal Sediments. *Cont. Shelf Res.* **2007**, *27*, 1174–1189. [CrossRef]
29. Ahmad, M.F.; Dong, P.; Mamat, M.; Nik, W.B.W.; Mohd, M.H. The Critical Shear Stresses for Sand and Mud Mixture. *Appl. Math. Sci.* **2011**, *5*, 53–71.
30. Winterwerp, J.C.; van Kesteren, W.G.M.; van Prooijen, B.; Jacobs, W. A Conceptual Framework for Shear Flow-Induced Erosion of Soft Cohesive Sediment Beds. *J. Geophys. Res. Ocean.* **2012**, *117*, C10020. [CrossRef]
31. Amos, C.L.; Daborn, G.; Christian, H.; Atkinson, A.; Robertson, A. In Situ Erosion Measurements on Fine-Grained Sediments from the Bay of Fundy. *Mar. Geol.* **1992**, *108*, 175–196. [CrossRef]
32. van Maren, D.S.; Cronin, K. Uncertainty in Complex Three-Dimensional Sediment Transport Models: Equifinality in a Model Application of the Ems Estuary, The Netherlands. *Ocean Dyn.* **2016**, *66*, 1665–1679. [CrossRef]
33. Agrawal, Y.C.; Pottsmith, H.C. Instruments for Particle Size and Settling Velocity Observations in Sediment Transport. *Mar. Geol.* **2000**, *168*, 89–114. [CrossRef]
34. Fugate, D.C.; Friedrichs, C.T. Determining Concentration and Fall Velocity of Estuarine Particle Populations Using Adv, Obs and Lisst. *Cont. Shelf Res.* **2002**, *22*, 1867–1886. [CrossRef]